

Efimov trimers under strong confinement

Jesper Levinsen,^{1,2} Pietro Massignan,³ and Meera M. Parish⁴

¹*Aarhus Institute of Advanced Studies, Aarhus University, DK-8000 Aarhus C, Denmark*

²*Cavendish Laboratory, JJ Thomson Avenue, Cambridge, CB3 0HE, United Kingdom*

³*ICFO - The Institute of Photonic Sciences - 08860 Castelldefels (Barcelona), Spain*

⁴*London Centre for Nanotechnology, Gordon Street, London, WC1H 0AH, United Kingdom*

(Dated: August 4, 2014)

The dimensionality of a system can fundamentally impact the behaviour of interacting quantum particles. Classic examples range from the fractional quantum Hall effect to high temperature superconductivity. As a general rule, one expects confinement to favour the binding of particles. However, attractively interacting bosons apparently defy this expectation: while three identical bosons in three dimensions can support an infinite tower of Efimov trimers, only two universal trimers exist in the two dimensional case. Here we reveal how these two limits are connected by investigating the problem of three identical bosons confined by a harmonic potential along one direction. We show that the confinement breaks the discrete Efimov scaling symmetry and successively destroys the weakest bound trimers. However, the deepest bound trimers persist even under strong confinement. In particular the ground state Efimov trimer hybridizes with the two-dimensional trimers, yielding a superposition of trimer configurations that effectively involves tunnelling through a short-range repulsive barrier. Our results suggest a way to use strong confinement to engineer more stable Efimov-like trimers, which have so far proved elusive.

I. INTRODUCTION

The quantum mechanical three-body problem displays surprisingly rich and complex behaviour despite its apparent simplicity. A fundamental example is the Efimov effect [1], which has intrigued physicists for decades owing to its peculiar and universal scaling properties. Its simplest incarnation only requires three bosons with resonant short-range interactions, and it can thus occur in a wide variety of systems ranging from nucleon systems [2] and ultracold atomic gases [3], to quantum magnets [4]. In particular, the cold-atom system finally provided the first experimental evidence for Efimov physics in 2006 [5], thus stimulating even greater interest in the subject.

A hallmark of the Efimov effect is a spectrum of three-body bound states (trimers) that exhibits a *discrete* scaling symmetry: for the simple case of three-dimensional (3D) identical bosons, the energy E of one trimer can be mapped onto another via the transformations $E \rightarrow \lambda_0^{-2n} E$ and $a \rightarrow \lambda_0^n a$, where a is the two-body scattering length, λ_0 is a known factor, and n is any integer [6]. In particular, at the unitarity point $1/a = 0$, the scattering length drops out of the problem and there exists an *infinite* number of weakly-bound s -wave trimer states [1], with the deepest bound trimer set by the short distance physics [6]. Such self-similar behaviour is reminiscent of more complex systems in Nature, such as coastlines, snow flakes and ferns [7], rather than of a typical few-body system — for instance, the two-body problem only exhibits a *continuous* scaling symmetry, where the low-energy properties simply scale with a . It is then natural to ask how these Efimov trimers evolve once the bosons are subject to confinement and the motion is constrained.

Cold-atom experiments already require the presence of a weak trapping potential, but the remarkable tunability of the atomic system has meant that more extreme

versions of confinement can now be realised, where one can create 2D Bose gases with markedly different many-body properties [8–10]. It is already known that the system dimensionality radically changes the few-boson problem: in 2D, the Efimov effect is absent [11] and only two s -wave trimers are predicted to exist, with universal energies $-16.5|E_b|$ and $-1.27|E_b|$ [12], where E_b is the two-body (dimer) binding energy. Here we show how this 2D limit evolves into Efimovian behaviour as we relax the confinement. We consider the simplest scenario of three identical bosons of mass m subjected to a tight harmonic confinement in the z -direction, $V(z) = \frac{1}{2}m\omega_z^2 z^2$, with confinement frequency ω_z . While the weakest bound Efimov trimers are successively destroyed with increasing confinement, crucially we find that the deepest states persist even for strong confinement. In particular, the ground state trimer is actually stabilised beyond its original regime of existence in 3D (Fig. 1). Moreover, in contrast to the dimer case, we obtain avoided crossings in the trimer spectrum. By evaluating the three-body hyperspherical potentials, we show that the avoided crossings correspond to trimer states that are superpositions of both short-range 3D-like and long-range 2D-like trimer configurations separated by a repulsive barrier. Such hybrid trimers could potentially be used to manufacture more stable Efimov-like trimers, thus paving the way for the exploration of many-body states of trimers.

II. THE QUASI-2D THREE-BOSON PROBLEM

The strong harmonic confinement described above is readily achieved in the cold-atom system via the application of an optical lattice or anisotropic trap [8–10]. Indeed, 2D-3D crossovers have already been investigated

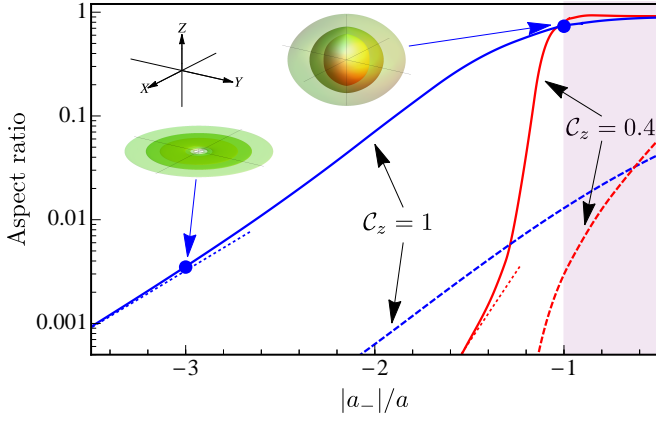


FIG. 1. Shape of the trimers under confinement: The aspect ratio $2\langle Z^2 \rangle / \langle \rho^2 \rangle$ for the two deepest trimers is shown as a function of interaction for two different confinement strengths C_z . Here ρ is the separation of an atom and a pair in the x - y plane, and Z is the separation in the confined direction (see main text). The deepest trimer (solid lines) only exists in 3D for $|a_-|/a \geq -1$, as depicted by the shaded region. Here the aspect ratio is close to 1, indicating that the trimer wavefunction resembles the 3D Efimov state. Outside the trimer's regime of existence in 3D, the aspect ratio quickly decreases, indicating that the trimer spreads out in the 2D plane. The change in aspect ratio as a crosses a_- is more gradual for the stronger confinement, due to a stronger coupling between trimers of a 2D and 3D character. The deepest trimer eventually approaches the 2D asymptotic limit (dotted lines, see Appendix D). A similar picture emerges for the first excited trimer (dashed lines), but the aspect ratio here is much smaller than 1 even away from the 2D limit. The shape of the deepest trimer is illustrated in the insets, which show surface density plots of the squared wavefunction (see the main text) evaluated at the points marked by filled circles.

in this manner in Fermi gases [13, 14]. For temperatures $T \ll \omega_z$ (we set $\hbar = k_B = 1$), non-interacting bosons will occupy the lowest harmonic oscillator level and will thus be kinematically 2D. However, in the presence of boson-boson interactions, the particles may virtually explore all excited states of the harmonic potential; thus we refer to the confined system as *quasi*-two-dimensional (q2D). An advantage of the harmonic potential is that one can decouple the centre-of-mass motion from the relative motion of the particles, so in the following we ignore the centre-of-mass contribution.

The effect of q2D confinement is twofold: it introduces an extra length scale, $l_z = \sqrt{1/m\omega_z}$, and it raises the threshold of the three-atom continuum from 0 to ω_z . Assuming that l_z and the scattering length a greatly exceed the van der Waals range of the interaction, the two-body problem is then completely parametrised by the dimensionless quantity l_z/a , and there is always a dimer bound state, in contrast to the 3D case. For weak attraction $l_z/a \ll -1$, we recover the 2D limit with dimer binding energy $E_b = -\frac{B}{m\pi l_z^2} e^{\sqrt{2\pi} l_z/a}$, where $B \approx 0.905$ [15], while for strong attraction $l_z/a \gg 1$ (or weak confine-

ment), this evolves into the 3D binding energy, $-1/ma^2$ (see Appendix A). The latter corresponds to the regime where the dimer is much smaller than the confinement length l_z and is therefore barely perturbed by the confinement.

The three-body problem, however, requires the additional length scale $1/\kappa_*$, which is set by the short-distance physics and fixes the 3D trimer energies in the resonant limit: $E_T^{(n)} \approx -\lambda_0^{-2n} \kappa_*^2/m$, with n a positive integer and $\lambda_0 \simeq 22.7$ [1]. A more natural quantity to consider in the cold-atom context is the scattering length $a_- < 0$ at which the deepest Efimov trimer crosses the three-atom continuum: this crossing leads to an enhanced three-body loss rate in the Bose gas, which is the main observable in experiment [5, 16–18]. Moreover, there is a remarkable universal relationship between a_- and the van der Waals range [19–21]. Thus, we characterise the three-body problem using the interaction parameter $|a_-|/a$ and the confinement parameter $C_z \equiv |a_-|/l_z$. Together, these determine how 2D or 3D a trimer is, as encoded in the aspect ratio displayed in Fig. 1. In particular, we see that when $|a_-|/a < -1$ (i.e. when there are no Efimov states in 3D), the two deepest trimers still persist under confinement and become substantially flattened within the x - y plane. Note that we only consider confinements $C_z \leq 1$, since $C_z \gg 1$ will make our results nonuniversal and sensitive to the details of the short-range interactions.

To determine the trimer wave functions and energies, we use the Skorniakov–Ter-Martirosian (STM) equation, first introduced in the context of neutron-deuteron scattering [22]. This takes advantage of the short-range nature of the two-body interaction to describe the three-body problem in terms of the relative motion of an atom and a pair. This equation has previously been extended to a q2D geometry for two species of fermions [23, 24]. In the case of three identical bosons, the STM equation for the q2D atom-pair vertex χ becomes

$$\begin{aligned} & \mathcal{T}^{-1}(\mathbf{k}_1, E_3 - \epsilon_{\mathbf{k}_1} - N_1 \omega_z) \chi_{\mathbf{k}_1}^{N_1} \\ &= 2 \sum_{\mathbf{k}_2, N_2, n_{23}, n_{31}} \frac{f_{n_{23}} f_{n_{31}} \langle N_1 n_{23} | N_2 n_{31} \rangle e^{-(k_1^2 + k_2^2)/\Lambda^2} \chi_{\mathbf{k}_2}^{N_2}}{E_3 - \epsilon_{\mathbf{k}_1} - \epsilon_{\mathbf{k}_2} - \epsilon_{\mathbf{k}_1 + \mathbf{k}_2} - (N_1 + n_{23}) \omega_z}. \end{aligned} \quad (1)$$

Here, the T-matrix \mathcal{T} describes the repeated interaction of two atoms, E_3 is the energy measured from the three-atom continuum threshold, and $\epsilon_{\mathbf{k}} = k^2/2m$. \mathbf{k}_i is the relative momentum of atom i with the pair (j, k) and we consider cyclic permutations of $(i, j, k) = (1, 2, 3)$. Defining the relative motion in the z -direction of two atoms, $z_{ij} = z_i - z_j$, and of an atom and a pair, $z_{i,jk} = \frac{z_j + z_k}{2} - z_i$, the corresponding harmonic oscillator quantum numbers are n_{ij} and N_i . Then $\langle N_1 n_{23} | N_2 n_{31} \rangle$ is the atom-pair Clebsch-Gordan coefficient, with selection rule $N_1 + n_{23} = N_2 + n_{31}$, and $f_{n_{ij}}$ is the relative

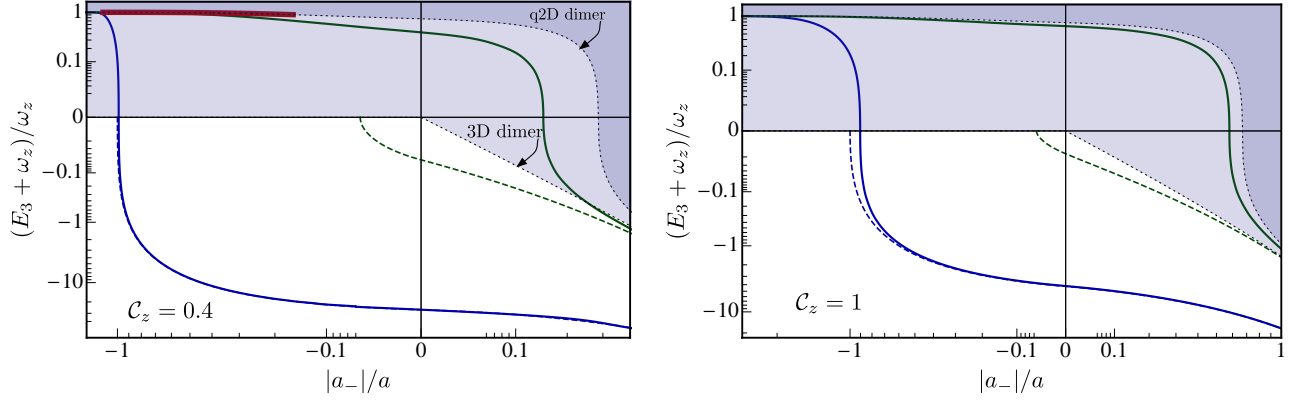


FIG. 2. Spectrum of trimers for two different confinement strengths. The q2D trimers are shown as solid lines, with energies $E_3 + \omega_z$ that take account of the raised three-atom continuum under confinement. For comparison, we also include the two deepest trimers in 3D (dashed lines). The shading illustrates the atom-dimer and three-atom continua, where the q2D continuum (contained within the 3D continuum) is shown with a darker shading. For a strong confinement with $C_z = 1$ (right), only two q2D trimers exist. For a weaker confinement with $C_z = 0.4$ (left), a third weakly bound trimer appears that is indistinguishable from the atom-dimer threshold on this scale; here we show its region of existence as a thick, red line on top of the threshold, but see Fig. 3 for a clearer rendering. In order to aid the visibility over the large energy range here, we rescaled the axes by means of the function $F_j(x) = \text{sgn}(x) \ln[1 + 5|x|^j]/\ln 6$, with $j = 1$ for the x -axis and $j = 1/2$ for the y -axis. For the 3D spectrum, ω_z is not defined and we display $ma_-^2 C_z^{-2} E_3$ as a function of $|a_-|/a$.

harmonic oscillator wavefunction at $z_{ij} = 0$. We include the short-distance physics by considering a two-body separable potential of the form $e^{-(k^2 + k'^2)/\Lambda^2}$, where Λ is an ultraviolet cutoff which fixes a_- (see Appendix B). Our results are independent of the specific choice of cutoff as long as the relevant length scales, $|a|$ and l_z , greatly exceed the short distance length scale $1/\Lambda$. This is the case for all results presented in this Article.

The q2D three-boson problem presents a considerable challenge, owing to the range of energy scales involved in the evolution towards Efimovian behaviour. Since the 3D spectrum possesses a discrete energy scaling of $22.7^2 \approx 515$, in practice, we require at least 515^3 Clebsch-Gordan coefficients after imposing the selection rule. However, the determination of these coefficients is greatly simplified once one realises that they can be related to Wigner's d -matrix [25] as follows:

$$\langle N_1 n_{23} | N_2 n_{31} \rangle = d_{\frac{N_2 - n_{31}}{2}, \frac{N_1 - n_{23}}{2}}^{\frac{N_1 + n_{23}}{2}} (2\pi/3). \quad (2)$$

To see this, first note that $\langle N_1 n_{23} | N_2 n_{31} \rangle$ is also the matrix element for the eigenstates of two isotropic 2D harmonic oscillators, related by a rotation in the plane by $\pi/3$. Then, using Schwinger's mapping [26], one defines angular momentum operators $\hat{\mathbf{J}} = \frac{1}{2} (\hat{b}_1^\dagger \hat{b}_2^\dagger) \hat{\sigma} \begin{pmatrix} \hat{b}_1 \\ \hat{b}_2 \end{pmatrix}$, with $\hat{\sigma}$ the usual Pauli spin matrices and \hat{b}_1, \hat{b}_2 harmonic oscillator operators. The eigenstates Θ of angular momentum are $|\Theta(j, m)\rangle = |N_1 n_{23}\rangle$, where $j = \frac{N_1 + n_{23}}{2}$ and $m = \frac{N_1 - n_{23}}{2}$ are the usual quantum numbers related to operators \hat{J}^2 and \hat{J}_z , respectively. In this basis, the rotation corresponds exactly to the application of $e^{-i(2\pi/3)\hat{J}_y}$, and thus we obtain Eq. (2).

III. TRIMER SPECTRA

The trimer energies E_3 are found as non-trivial solutions of Eq. (1), and the complete spectra are displayed in Figs. 2 and 3. We see immediately that the extra length scale l_z removes the weakest bound Efimov states, similarly to the effect of a finite scattering length in 3D. In particular, l_z may be interpreted as a large distance cut-off, since Efimov trimers much larger than this will be strongly perturbed by the confinement. Consequently, a discrete scaling symmetry only exists for scattering lengths in the range $|a_-| \ll |a| \ll l_z$. Thus, for the moderate to strong confinements considered here, where $l_z \sim |a_-|$, the symmetry is clearly broken.

Figure 2 shows a comparison between our q2D spectra and the universal 3D results. For increasing $|a_-|/a$, we see that the ground state trimer eventually resembles the 3D result even when subjected to a strong confinement, $C_z = 1$, which is consistent with the approximately spherical shape of the trimer in Fig. 1. This is reasonable since the properties of the deepest trimer in 3D are set by short-distance physics: universal theory predicts the size to be of order $|a_-|$ for negative scattering lengths $|a_-|/a > -1$ [6], and thus the deepest trimer will only be weakly perturbed by the confinement when $C_z \lesssim 1$. Another key feature of the q2D spectrum is the raised threshold for free atom motion compared with the 3D case. As expected, the trimers are significantly affected by the confinement when their energies are well above the 3D threshold. However, note that the binding energy of the ground state trimer can still be a substantial fraction of ω_z when $|a_-|/a \sim -1$, and thus the trimer should be

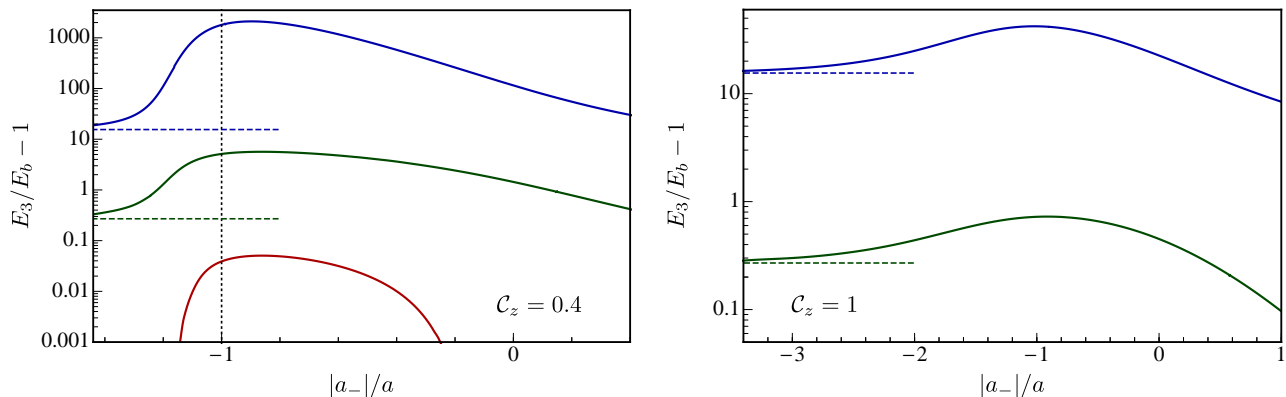


FIG. 3. Ratio between q2D trimer and dimer energies. The trimer energies (solid lines) are displayed as a function of interaction for two different confinements: $C_z = 0.4$ (left) and $C_z = 1$ (right). In the limit $|a_-|/a \lesssim -1$, the trimer energies converge to the universal 2D results $-16.5|E_b|$ and $-1.27|E_b|$ [12] (dashed lines). For moderate confinement (left), we see evidence of an avoided crossing resulting from the coupling between three ‘bare’ states: the two 2D trimers, and a third trimer which emerges from the continuum at $a \simeq a_-$ (vertical dotted line).

resistant to thermal dissociation when $T \ll \omega_z$.

Remarkably, the raised q2D continuum threshold also stabilizes the two deepest trimers for weak interactions, as clearly seen in Fig. 3. This results from the fact that the trimers in 2D and 3D have the same s -wave symmetry and thus Efimov trimers can smoothly evolve into long-range 2D-like trimers, without any level crossings. In the regime $|a_-|/a < -1$, i.e., where no trimers exist in 3D, we observe how a continuous scaling symmetry is recovered and the trimer energies approach the universal 2D results. For sufficiently weak confinement, we even obtain avoided crossings, as clearly observed in Fig. 3 when $C_z = 0.4$: here, a third trimer appears for a scattering length close to a_- , a remnant of the crossing of the deepest trimer with the continuum in 3D. This suggests that we can have a superposition of 2D and 3D-like trimers; this is made possible by the presence of a repulsive barrier (see Fig. 4), as we discuss below. The third trimer state is very weakly bound for $C_z = 0.4$ and is expelled into the continuum as the strength of the confinement is increased. Once $C_z \gtrsim 0.6$, the third trimer disappears along with any pronounced avoided crossings.

IV. THREE-BODY POTENTIALS AND TRIMER WAVEFUNCTIONS

Considerable insight into the q2D spectra can be gained from the adiabatic hyperspherical approach. This has been developed for both 3D [6, 27] and 2D [28], and in Appendix C we describe how this framework can be suitably adapted to the intermediate q2D system. The hyperspherical approach allows us to determine an effective three-body potential $V(R)$, where the hyperradius $R^2 = r_1^2 + r_2^2 + r_3^2$ is defined in terms of the atom positions \mathbf{r}_i at vanishing centre-of-mass coordinate. The potential appears in an effective hyperradial Schrödinger equation

$[-(1/2m)\partial^2/\partial R^2 + V(R)]f_0(R) = (E_3 + \omega_z)f_0(R)$, where we ignore all but the lowest scattering channel, an approximation valid in the 3D regime $R < l_z$, both when $R \ll |a|$ and $R \gg |a|$. For all other R , this should at least provide a qualitative description — in particular, we recover 2D behaviour when $R \gg l_z$. Note that $V(R)$ depends only on l_z/a and makes no reference to the three-body parameter. Therefore, one needs to supplement this with a short-distance boundary condition on the wavefunction, which is equivalent to fixing Λ or $|a_-|$.

We show in Fig. 4 our calculated q2D hyperspherical potentials for $|a_-|/a < 0$. At short distances, $V(R)$ matches the 3D potential, which is attractive $\sim 1/R^2$ for $R \ll |a|$. On the other hand, when $R \rightarrow \infty$, the effects of confinement become apparent and $V(R) \rightarrow \omega_z - |E_b|$, corresponding to the free motion of an atom and a dimer within the plane. When $l_z/a \lesssim -2.5$, the potential also features a barrier at intermediate radii $R \approx |a|$, with height $\sim 0.15/ma^2$. Approaching the limit $l_z/a \ll -1$, we see that $V(R)$ at $R \gg l_z$ resembles the 2D hyperspherical potential [28], which features a centrifugal repulsion and a long-range attractive tail with respect to the continuum. This attraction gives rise to the two trimer states that exist for arbitrarily weak interactions, unlike the Efimov trimers in 3D. Note that this differs from the three-body problem under *isotropic* harmonic confinement [29–32], where we expect $V(R) \sim R^2$ for large R .

The presence of a repulsive barrier in the hyperspherical potential means that trimer resonances at short distances can exist. This same feature is responsible for the loss resonances in 3D when $a \sim a_-$. For moderate q2D confinement (e.g., $C_z = 0.4$ as shown in Fig. 4), it gives rise to a superposition of short-range 3D-like and long-range 2D-like trimer configurations. This is best

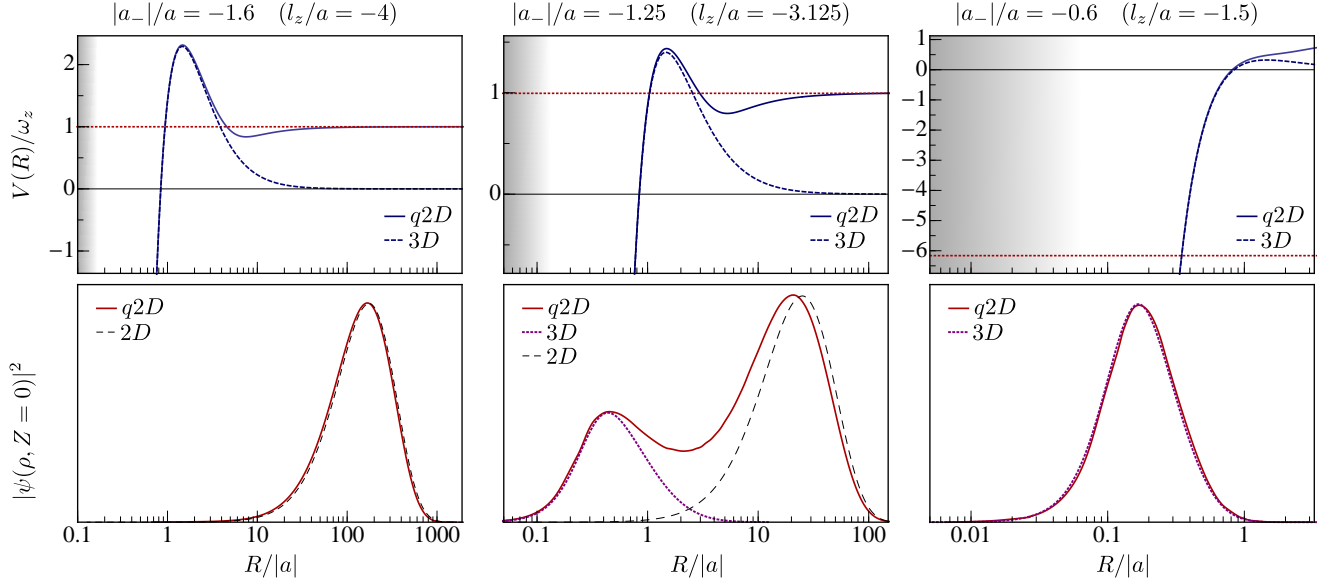


FIG. 4. Three-body potentials and corresponding wavefunctions of the deepest trimer. The upper panels show the q2D adiabatic hyperspherical potential $V(R)$ for three different interactions $|a_-|/a$, assuming $C_z = 0.4$. For reference, we also show the 3D potential. Note that the potentials match in the region $R < l_z$. The shaded area corresponds to the regime of short-distance physics where R is less than the van der Waals range $\sim 1/\Lambda$. The resulting energies of the ground state trimer are shown as dashed horizontal lines. In the lower panels, the in-plane q2D probability densities $|\psi(\rho, Z=0)|^2$ are compared with the probability densities expected in purely 2D and 3D. This illustrates three qualitatively different interaction regimes: (left), for weak interactions, the trimer resides in the long-range attractive tail of the potential and matches the 2D result; (centre), for intermediate interactions, $a \sim a_-$, the trimer configuration is a superposition of trimers of 2D and 3D character. Here, as there is no Efimov trimer at this scattering length in 3D, the 3D probability density is instead evaluated at $|a_-|/a$ slightly larger than -1. (Right), for stronger interactions $|a_-|/a > -1$ the trimer wavefunction resides mainly in the regime $R < |a|$ and closely resembles the 3D wavefunction.

illustrated by considering the wavefunction $\psi(\boldsymbol{\rho}, Z) \equiv R^{3/2} \sum_{\mathbf{k}, N} e^{i\mathbf{k} \cdot \boldsymbol{\rho}} \phi_N(Z) \chi_{\mathbf{k}}^N$, describing the relative motion of an atom with a pair. Here, $\boldsymbol{\rho}$ is the atom-pair separation in the plane, Z is the separation in the transverse direction, and $\phi_N(Z)$ is the harmonic oscillator wavefunction of a particle of mass $2m/3$, the reduced mass of the atom-pair system. Note, in particular, that the probability distribution $|\psi(\boldsymbol{\rho}, Z)|^2$ reduces to $|f_0(R)|^2$ in the 3D limit (up to normalisation factors), where $R^2 = \frac{2}{3}(\rho^2 + Z^2)$.

Figure 4 clearly illustrates that the wavefunction of the deepest trimer exhibits both 2D and 3D-like components once a approaches a_- and a trimer resonance in the 3D potential appears. This hybridisation of trimer configurations is, in turn, connected with the avoided crossings observed in Fig. 3. With increasing interaction, the deepest trimer evolves into an Efimov-like trimer that resides at short distances $R < |a|$. This evolution from 2D to 3D behaviour is mirrored by the aspect ratio $2\langle Z^2 \rangle / \langle \rho^2 \rangle$ (see Appendix D) in Fig. 1. In general, we expect to encounter a 2D-3D trimer hybridisation every time a 3D trimer resonance appears behind the potential barrier. Thus, if we were to relax the confinement until $C_z < 1/22.7$, the scenario depicted in Fig. 4 would similarly occur for the second deepest trimer.

V. CONSEQUENCES FOR BOSE GAS EXPERIMENTS IN CONFINED GEOMETRIES

We now discuss the ramifications of our results for current cold-atom experiments. For definiteness, we consider ^{133}Cs , the first atomic species in which Efimov physics was observed [5]. In this case, $a_- \simeq -957a_0$ [19], where a_0 is the Bohr radius, so that $C_z = 1$ corresponds to a confinement frequency of $\omega_z \simeq 2\pi \times 30\text{kHz}$. While frequencies close to 100kHz have been used for side-band cooling of ^{133}Cs [33, 34], such strong confinement is far from common in experiments investigating low-dimensional physics. Indeed, scale invariance and universality in the repulsive 2D Bose gas were investigated using a confinement $\omega_z \simeq 2\pi \times 1.9\text{kHz}$, corresponding to $C_z \simeq 0.25$ [10]. Thus we expect that in realistic q2D experiments, the energy of the deepest trimer will typically resemble the universal 3D case.

On the other hand, the raised three-atom continuum under confinement will strongly impact the 3D Efimov loss features in the three-atom scattering. In particular, there can no longer be any trimer loss resonances once ω_z exceeds the height of the repulsive barrier in the hyperspherical potential — we estimate this to occur when $l_z/a \simeq -2.5$. Thus, we expect the loss peak of the deepest trimer to disappear for confinements $C_z =$

$|a_-|/l_z \gtrsim 0.4$. Likewise, universality dictates that the peak associated with the next Efimov state disappears when $C_z \gtrsim 0.4/22.7$. For the case of ^{133}Cs , this latter value corresponds to a confinement of $\omega_z \simeq 2\pi \times 9\text{Hz}$, indicating that a very weak trapping potential is needed in order to observe the second Efimov peak. Note, further, that these arguments translate in a generic manner to all geometries; one simply needs to compare the height of the repulsive barrier at the 3D Efimov loss resonance to the increase in the three-atom continuum. Consequently, our findings have implications for any experiment seeking to detect shallow trimers in a trap, and hence the quest to observe true Efimov scaling in an ultracold atomic gas.

To experimentally probe our q2D spectra in Figs. 2 and 3, one could associate trimers using a radio frequency pulse. In 3D, this has successfully been applied by driving transitions in the internal states of the atoms [35] or by modulating the magnetic field [36]. However, in contrast to 3D, the resulting trimers in the strongly confined geometry may be relatively long lived: hybrid trimers in the regime $a \sim a_-$ only have a small weight in the short distance region (see Fig. 4), resulting in a reduced overlap with deeply bound (non-universal) states. Accordingly, collisional relaxation into deeper states (the main loss mechanism in 3D) will be suppressed.

VI. CONCLUSIONS AND OUTLOOK

A priori, there is no reason to believe that the physical picture presented here should apply uniquely to three identical bosons in a q2D geometry. For instance, we expect a trimer spectrum similar to those of Figs. 2 and 3 to occur in a q1D geometry — theoretically this may be studied by including all confinement levels instead of simply projecting onto the lowest level as in Ref. [37]. Likewise, while two tetramers have been predicted [38] and observed [39] to accompany each Efimov trimer in 3D, exactly two universal tetramers are predicted to exist in 2D [40]. Consequently, we expect a spectrum which displays avoided crossings between tetramers of 2D and 3D character, while the two deepest tetramers are stabilized by the application of a strong confinement. An important implication of our work is thus that, under realistic experimental conditions, three- and four-body correlations in the q1D and q2D Bose gas may be strongly affected by Efimov physics, i.e., markedly different from predictions of universal 1D and 2D theory.

Finally, our work suggests that strong q2D confinement could be used to engineer more stable, Efimov-like, hybrid trimers owing to the presence of a repulsive barrier and the associated small weight of the trimer wavefunction at small distances. In particular, our results are also applicable to three distinguishable *fermions* with approximately equal interspecies interactions, as can be the case with ^6Li atoms [35]. This may allow for the formation of a many-body state of long-lived trimers, an important goal which has so far remained elusive in the context of

ultracold experiments.

ACKNOWLEDGMENTS

We gratefully acknowledge fruitful discussions with M. Berninger, E. Braaten, F. Ferlaino, R. Grimm, B. Huang, V. Ngampruetikorn, D. S. Petrov, M. Zaccanti and A. Zenesini. JL and PM wish to acknowledge support from POLATOM. JL further acknowledges support from the Carlsberg Foundation, PM from ERC AdG OSYRIS, EU EQuaM, and Fundació Cellex, while MMP acknowledges support from the EPSRC under Grant No. EP/H00369X/2.

Appendix A: Hamiltonian and two-body problem

The Hamiltonian in the absence of confinement is chosen to be

$$\mathcal{H} = \sum_{\mathbf{k}} \epsilon_{\mathbf{k}} \hat{a}_{\mathbf{k}}^\dagger \hat{a}_{\mathbf{k}} + \frac{g}{2} \sum_{\mathbf{k}_1, \mathbf{k}_2, \mathbf{k}_3} \xi(k_{12}) \xi(k_{34}) \hat{a}_{\mathbf{k}_1}^\dagger \hat{a}_{\mathbf{k}_2}^\dagger \hat{a}_{\mathbf{k}_3} \hat{a}_{\mathbf{k}_4},$$

where $\hat{a}_{\mathbf{k}}$ ($\hat{a}_{\mathbf{k}}^\dagger$) is the annihilation (creation) operator of atoms with momentum \mathbf{k} , $\mathbf{k}_{ij} \equiv \frac{\mathbf{k}_i - \mathbf{k}_j}{2}$ is the relative momentum, and $\mathbf{k}_4 = \mathbf{k}_1 + \mathbf{k}_2 - \mathbf{k}_3$. $\xi(k)$ is a function describing the cutoff of the interaction at large momenta, and we take this to be $\xi(k) = e^{-k^2/\Lambda^2}$.

The two-body T-matrix appearing in the STM equation describes scattering of two atoms with total planar momentum \mathbf{k} and energy E measured from the two-atom continuum. It takes the form

$$\mathcal{T}(\mathbf{k}, E) = \frac{2\sqrt{2\pi}}{m} \left\{ \frac{l_z}{a} - \mathcal{F} \left(\frac{-E + k^2/4m}{\omega_z} \right) \right\}^{-1}.$$

Here, the interaction is renormalized by the use of the 3D scattering length a . For a Gaussian cutoff, we obtain

$$\mathcal{F}(x) = \int_0^\infty du \frac{1 - \frac{e^{-xu}}{\sqrt{[(1+\lambda)^2 - (1-\lambda)^2 e^{-2u}]/(2u+4\lambda)}}}{\sqrt{4\pi(u+2\lambda)^3}},$$

with $\lambda \equiv (l_z \Lambda)^{-2}$. Our expression for \mathcal{F} reduces to that of Ref. [41] in the limit $\lambda \rightarrow 0$. The dimer binding energy E_b measured from the continuum is defined through $l_z/a = \mathcal{F}(-E_b/\omega_z)$.

In our model, the wavefunctions of the relative motion evaluated at the origin are

$$f_{n_r} = (-1)^{n_r/2} \sqrt{\frac{(n_r-1)!!}{n_r!!}} \frac{1}{\sqrt{1+\lambda}} \left(\frac{1-\lambda}{1+\lambda} \right)^{n_r/2},$$

if n_r is even, and 0 otherwise (we absorbed the prefactor $(m\omega_z/2\pi)^{1/4}$ into the definition of \mathcal{T}).

Appendix B: Three-body problem

In Eq. (1) we employ the simplification $\xi(\mathbf{k}_1 + \mathbf{k}_2/2)\xi(\mathbf{k}_2 + \mathbf{k}_1/2) \rightarrow \xi(k_1)\xi(k_2)$ in the 2D plane. This allows us to project the equation analytically onto the s -wave, $\chi_{k_1}^{N_1} \equiv \int \frac{d\phi}{2\pi} \chi_{\mathbf{k}_1}^{N_1}$, where ϕ is the angle of \mathbf{k}_1 with some axis. Once Λ has been used to fix the three-body parameter, the physics at energy scales much smaller than Λ^2/m becomes insensitive to this change. Using the 3D STM equation with our two-body interaction, for the deepest Efimov trimer we find the energy $-0.05\Lambda^2/m$ at the Feshbach resonance and $a_- = -9.39/\Lambda$. Since the trimer energies considered in the q2D geometry are always smaller than those in the 3D geometry (see Fig. 2), the assumption that we consider energies much smaller than Λ^2/m is well justified.

Appendix C: Hyperspherical approach in q2D

Beginning with the Jacobi coordinates $\mathbf{r}_{ij} = \mathbf{r}_i - \mathbf{r}_j$ and $\mathbf{r}_{k,ij} = \frac{1}{2}(\mathbf{r}_i + \mathbf{r}_j) - \mathbf{r}_k$, and assuming that $\mathbf{r}_1 + \mathbf{r}_2 + \mathbf{r}_3 = 0$, the hyperradius corresponds to $R^2 = \frac{1}{2}r_{ij}^2 + \frac{2}{3}r_{k,ij}^2$, while the transformation $r_{ij} = \sqrt{2}R \sin \alpha_k$, $r_{k,ij} = R\sqrt{\frac{3}{2}} \cos \alpha_k$ defines the hyperangle α_k . Following Ref. [6], we use the hyperspherical expansion of the wave function: $\Psi(R, \Omega) = \frac{1}{R^{5/2} \sin(2\alpha_k)} \sum_{n=0}^{\infty} f_n(R) \Phi_n(R, \Omega)$. Here, the angular quantity $\Omega = (\alpha_k, \theta_{ij}, \theta_{k,ij})$, where the projections $\hat{\mathbf{r}}_{ij} \cdot \hat{\mathbf{z}} = \cos \theta_{ij}$, $\hat{\mathbf{r}}_{k,ij} \cdot \hat{\mathbf{z}} = \cos \theta_{k,ij}$, and we assume that Ψ is approximately independent of the azimuthal angles. We now further expand the angular function $\Phi_n(R, \Omega) = \sum_{\mathbf{m}} \eta_{n\mathbf{m}}(R, \alpha_k) h_{\mathbf{m}}(R, \Omega)$, with $\mathbf{m} = (m_1, m_2)$ a set of non-negative integers. Writing

$h_{\mathbf{m}} = \tau_{m_1}(R \sin \alpha_k, \theta_{ij}) \times \tau_{m_2}(R \cos \alpha_k, \theta_{k,ij})$, the function $\tau(X, \theta)$ obeys the equation

$$\left[-\frac{l_z^2}{X^2} \frac{1}{\sin \theta} \frac{\partial}{\partial \theta} \left(\sin \theta \frac{\partial}{\partial \theta} \right) + \frac{X^2}{l_z^2} \cos^2 \theta \right] \tau = 2\mu\tau$$

where μ is an eigenvalue that is independent of θ , and $X = R \cos \alpha_k$ or $X = R \sin \alpha_k$, depending on whether we consider $\theta_{k,ij}$ or θ_{ij} . In the limit $X \ll l_z$, τ yields the Legendre polynomials expected in the 3D case, while in the opposite limit $X \gg l_z$, τ evolves into the harmonic oscillator wavefunctions of the q2D confinement. Finally we use μ to solve the equation for η_{00} and obtain the lowest hyperspherical potential $V(R)$ in the usual way within the adiabatic hyperspherical approximation [6].

Appendix D: Aspect ratio of trimers

The wavefunction can in general be decomposed in its Fadeev components $\Psi(\mathbf{r}_1, \mathbf{r}_2, \mathbf{r}_3) = \psi^{(1)}(\mathbf{r}_{23}, \mathbf{r}_{1,23}) + \psi^{(2)}(\mathbf{r}_{13}, \mathbf{r}_{2,31}) + \psi^{(3)}(\mathbf{r}_{12}, \mathbf{r}_{3,12})$. Here $\psi^{(1)}(\mathbf{r}_{23}, \mathbf{r}_{1,23})$ is the real space form of the function $\psi_{\mathbf{k}_{23}, \mathbf{k}_1, n_{23}, N_1}^{(1)} \propto \frac{f_{n_{23}} \chi_{\mathbf{k}_1}^{N_1}}{E_3 - k_{23}^2/m - 3k_1^2/4m - (n_{23} + N_1)\omega_z}$. We then calculate the aspect ratio of the relative atom-pair coordinate, assuming that cross terms may be neglected:

$$\frac{2\langle z_{1,23}^2 \rangle}{\langle \rho_{1,23}^2 \rangle} = \frac{2 \int d^2 \rho_{23} d^2 \rho_{1,23} dz_{23} dz_{1,23} z_{1,23}^2 |\psi^{(1)}(\mathbf{r}_{23}, \mathbf{r}_{1,23})|^2}{\int d^2 \rho_{12} d^2 \rho_{1,23} dz_{23} dz_{1,23} \rho_{1,23}^2 |\psi^{(1)}(\mathbf{r}_{23}, \mathbf{r}_{1,23})|^2}.$$

When $|a_-|/a \ll -1$, the aspect ratio approaches the 2D limit where $\langle z_{1,23}^2 \rangle = 3l_z^2/4$ and $\langle \rho_{1,23}^2 \rangle = 0.037/(m|E_b|)$.

-
- [1] V. Efimov, Phys. Lett. B **33**, 563 (1970).
 - [2] V. Efimov, Sov. J. Nucl. Phys. **12**, 589 (1971).
 - [3] F. Ferlaino *et al.*, Few-Body Systems **51**, 113 (2011).
 - [4] Y. Nishida, Y. Kato, and C. D. Batista, Nature Phys. **9**, 93 (2013).
 - [5] T. Kraemer *et al.*, Nature **440**, 315 (2006).
 - [6] E. Braaten and H.-W. Hammer, Physics Reports **428**, 259 (2006).
 - [7] B. Mandelbrot, *The Fractal Geometry of Nature* (Henry Holt and Company, New York, 1983).
 - [8] Z. Hadzibabic *et al.*, Nature **441**, 1118 (2006).
 - [9] P. Cladé *et al.*, Phys. Rev. Lett. **102**, 170401 (2009).
 - [10] C.-L. Hung, X. Zhang, N. Gemelke, and C. Chin, Nature **470**, 236 (2011).
 - [11] Y. Nishida and S. Tan, Few-Body Systems **51**, 191 (2011).
 - [12] L. W. Bruch and J. A. Tjon, Phys. Rev. A **19**, 425 (1979).
 - [13] A. T. Sommer *et al.*, Phys. Rev. Lett. **108**, 045302 (2012).
 - [14] K. Günter *et al.*, Phys. Rev. Lett. **95**, 230401 (2005).
 - [15] D. S. Petrov and G. V. Shlyapnikov, Phys. Rev. A **64**, 012706 (2001).
 - [16] M. Zaccanti *et al.*, Nature Phys. **5**, 586 (2009).
 - [17] N. Gross, Z. Shotan, S. Kokkelmans, and L. Khaykovich, Phys. Rev. Lett. **103**, 163202 (2009).
 - [18] S. E. Pollack, D. Dries, and R. G. Hulet, Science **326**, 1683 (2009).
 - [19] M. Berninger *et al.*, Phys. Rev. Lett. **107**, 120401 (2011).
 - [20] S. Roy *et al.*, Phys. Rev. Lett. **111**, 053202 (2013).
 - [21] J. Wang, J. P. D'Incao, B. D. Esry, and C. H. Greene, Phys. Rev. Lett. **108**, 263001 (2012).
 - [22] G. V. Skorniakov and K. A. Ter-Martirosian, Sov. Phys. JETP **4**, 648 (1957).
 - [23] J. Levinsen, T. G. Tiecke, J. T. M. Walraven, and D. S. Petrov, Phys. Rev. Lett. **103**, 153202 (2009).
 - [24] J. Levinsen and M. M. Parish, Phys. Rev. Lett. **110**, 055304 (2013).
 - [25] E. P. Wigner, *Group Theory and Its Application to the Quantum Mechanics of Atomic Spectra* (Academic Press, New York, 1959).
 - [26] J. Schwinger, in *Quantum Theory of Angular Momentum*, edited by L. C. Biedenharn and H. van Dam (Academic Press, New York, 1965), pp. 229–279.

- [27] E. Nielsen, D. V. Fedorov, A. S. Jensen, and E. Garrido, *Physics Reports* **347**, 373 (2001).
- [28] E. Nielsen, D. V. Fedorov, and A. S. Jensen, *Few-Body Systems* **27**, 15 (1999).
- [29] S. Jonsell, H. Heiselberg, and C. J. Pethick, *Phys. Rev. Lett.* **89**, 250401 (2002).
- [30] F. Werner and Y. Castin, *Phys. Rev. Lett.* **97**, 150401 (2006).
- [31] M. Thøgersen, D. V. Fedorov, and A. S. Jensen, *Phys. Rev. A* **78**, 020501 (2008).
- [32] J. Portegies and S. Kokkelmans, *Few-Body Systems* **51**, 219 (2011).
- [33] V. Vuletić, A. J. Kerman, C. Chin, and S. Chu, *Phys. Rev. Lett.* **82**, 1406 (1999).
- [34] I. Bouchoule *et al.*, *Phys. Rev. A* **59**, R8 (1999).
- [35] T. Lompe *et al.*, *Science* **330**, 940 (2010).
- [36] O. Machtey, Z. Shotan, N. Gross, and L. Khaykovich, *Phys. Rev. Lett.* **108**, 210406 (2012).
- [37] C. Mora, R. Egger, and A. O. Gogolin, *Phys. Rev. A* **71**, 052705 (2005).
- [38] J. von Stecher, J. P. D’Incao, and C. H. Greene, *Nature Physics* **5**, 417 (2009).
- [39] F. Ferlino *et al.*, *Phys. Rev. Lett.* **102**, 140401 (2009).
- [40] L. Platter, H.-W. Hammer, and U.-G. Meißner, *Few-Body Systems* **35**, 169 (2004).
- [41] I. Bloch, J. Dalibard, and W. Zwerger, *Rev. Mod. Phys.* **80**, 885 (2008).